Spatio-temporal characterisation of a 100 kHz 24 W sub-3-cycle NOPCPA laser system

OPEN ACCESS
IOP Publishing
Journal of Optics
J. Opt. **20** (2018) 044003 (8pp)
https://doi.org/10.1088/2040-8986/aaadc3

Spatio-temporal characterisation of a 100 kHz 24 W sub-3-cycle NOPCPA laser system

Tobias Witting, Federico J Furch and Marc J J Vrakking

Max Born Institute for Nonlinear Optics and Short Pulse Spectroscopy, Max-Born-Straße 2a, D-12489, Berlin, Germany

E-mail: witting@mbi-berlin.de

Received 7 September 2017, revised 25 January 2018
Accepted for publication 8 February 2018
Published 26 February 2018

Abstract

In recent years, OPCPA and NOPCPA laser systems have shown the potential to supersede Ti:sapphire plus post-compression based laser systems to drive next generation attosecond light sources via direct amplification of few-cycle pulses to high pulse energies at high repetition rates. In this paper, we present a sub 3-cycle, 100 kHz, 24 W NOPA laser system and characterise its spatio-temporal properties using the SEA-F-SPIDER technique. Our results underline the importance of spatio-temporal diagnostics for these emerging laser systems.

Keywords: ultrafast metrology, ultrafast technology, OPCPA, NOPA, NOPCPA

(Some figures may appear in colour only in the online journal)

1. Introduction

The availability of carrier-envelope-phase (CEP) stable few- to single-cycle laser pulses [1] with sufficient pulse energy to efficiently drive high-order harmonic generation (HHG) combined with suitable gating techniques to isolate attosecond pulses from HHG has led to the creation and rapid growth of the field of attosecond science [2].

Most driver laser systems are based on mJ-level Ti:sapphire-based chirped pulse amplification (CPA) systems with active CEP stabilisation. State of the art pulse durations are in the 30 fs range with pulse energies ranging from 1 mJ to multiple mJ at repetition rates of one to a few kHz. In order to efficiently generate isolated attosecond laser pulses by means of HHG, the pulses have to be compressed. The combination of a Ti:sapphire CPA system and nonlinear post-compression [3] is now well established. Especially, pulse compression in gas-filled hollow capillaries is a robust route to the day-to-day availability of few- to near single-cycle laser pulses with good CEP stability [4]. Typically, pulse energies of the few-cycle pulses range from hundreds of μJ to a few mJ [5, 6] at repetition rates of one to a few kHz. Recent interesting developments include self-compression in Kagome photonic crystal fibres for extremely compact single- or even sub-cycle laser sources with modest pulse energy [7], as well as coherent combination with the aim to reach 10 or more mJ level pulses [8].

The aforementioned Ti:sapphire CPA laser systems with post-compression are combined with high harmonic generation in gases to generate phase-locked attosecond pulse trains. In order to generate isolated attosecond pulses (IAPs), a suitable gating technique needs to be employed. IAPs in the 30–40 eV region can be generated via polarisation gating [9]. IAPs produced by pure amplitude gating have been generated near the cut-off of the HHG spectrum [10]. Amplitude gating also enabled the simultaneous generation of sub-fs VUV and attosecond XUV pulses [11]. Double optical gating enabled the generation of attosecond pulses with durations down to 67 as [12]. HHG in ablation plasma plumes has also lead to the gating of IAPs when media with resonances are employed [13]. The combination of Ti:sapphire amplifiers with post-compression and attosecond pulse generation has enabled pump-probe experiments with attosecond temporal resolution.

Attosecond science is now a mature research field [14]. Attosecond resolution pump-probe experiments have been performed in a number of atomic [15, 16], molecular [17], and solid state [18–20] systems. Usual observables in these experiments are kinetic energy distributions of electrons and/or ions or the transient absorption of the XUV radiation. However, in order to extend attosecond science to more complex systems, it would be desirable to record the full electron and ion three-dimensional momentum distributions in coincidence using a reaction microscope [21]. As the event rate has to be kept at a fraction of the laser repetition rate to ensure single events per laser shot, the typical repetition rate of Ti:sapphire plus post-compression attosecond drive laser technology in the order of one to a few kHz is a severe limitation. The highest reported repetition rate is 10 kHz [22]. To move from proof-of-principle experiments to the investigation of more complex systems much higher laser repetition rates are necessary.

Currently two branches of laser technology have emerged that deliver few-cycle laser pulses with repetition rates in the hundreds of kHz to MHz range, namely fibre-based laser systems, and non-collinear optical parametric chirped pulse amplifiers (NOPCPAs). Fibre-based laser systems offer high repetition rates in compact setups but require aggressive (multi-stage) post-compression to reach few-cycle pulses [23] and CEP stability has so far not been demonstrated. NOPCPAs are a very attractive route to energetic few-cycle pulses at high repetition rates. High gains over a broad gain bandwidth can be achieved. As the amplification process is instantaneous, NOPCPAs do not suffer from thermal effects in the same way that traditional laser amplifiers do, and are therefore ideally suited for high average power applications. Few-cycle, high ($\geqslant$100 kHz) repetition rate NOPCPAs around 800 nm wavelength utilising Ti:sapphire oscillators as front-ends have been demonstrated for a wide range of pulse energies, repetition rates and average powers [24–27]. Recently, we have been able to demonstrate amplification of CEP stable 7 fs pulses to average powers of 24 W at 100 kHz repetition rate [28].

In this paper, we first describe our NOPCPA laser system, introduce spatio-temporal metrology methods with a focus on the SEA-F-SPIDER device, and finally report spatio-temporal measurements of the NOPCPA laser system.

2. NOPCPA laser system

Our NOPCPA laser system is based around a Ti:sapphire oscillator front-end. The oscillator (Venteon Pulse:One) has an octave spanning spectrum, which enables compression to few-cycle duration, low noise CEP locking with residual rms phase noise of 150 mrad, as well as direct seeding of the pump laser chain for the NOPAs by splitting off an approximately 10 nm wide part of the spectrum at 1030 nm with a dichroic mirror and bandpass filter.

A schematic of the system is shown in figure 1. The 1030 nm output of the oscillator is coupled into a polarisation-maintaining fibre and pre-amplified in an Yb:fibre amplifier. Stretching is achieved with a fibre Bragg grating stretcher. The main amplification occurs in a thin disk Yb:YAG regenerative amplifier (DIRA200, Trumpf Scientific GmbH). This laser provides an average power of 220 W at 100 kHz repetition rate. After compression in a grating compressor, up to 190 W in 1.1 ps pulses are available at 1030 nm. These pulses are frequency doubled to 515 nm in a second harmonic generation stage. Up to 120 W average power with pulses of 900 fs duration are available to pump the NOPA amplification stages. We use a system of half-wave retarders and thin-film polarisers to distribute the pump beam to the delay stabilisation system (DSS), and to the first and second stage non-collinear amplification stages.

The main output of the oscillator passes through a 4-f-line pulse shaper (PS) (Biophotonics Solutions Inc., MIIPS Box 640P), which enables tuning of higher order phase terms for optimal pulse compression. The seed pulses are stretched to approximately 300 fs at this point. After spatial filtering, the seed beam is sent to the amplification stages. A fraction is split off send sent to a DSS. In this unit, we use a fraction of the pump beam to pump a NOPA stage with the seed beam additionally stretched by 5 cm of SF11. Due to the chirp of the seed pulse in the DSS the amplified signal wavelength depends on the timing between seed and pump laser beams. The concept is similar to that reported in [29], but all signal processing is done digitally in our system. We use a fibre-coupled spectrometer (Flame-S-VIS-NIR, Ocean Optics) to monitor the amplified spectrum. We use numerical cross-correlation with a reference spectrum to derive a feedback signal. A translation stage is used to set the time delay of the seed beam. We use a small mass piezo stage (PI) for fast ($\sim$110 Hz) feedback and a DC motor-driven stage with 50 mm range for long-term timing drift correction. With this dual stage system we can keep the time delay between seed and pump pulses locked over an entire day to rms values of 2.5 fs. Apart from active locking, the PC based system also allows for controlled adjustments of the time delay, which is convenient for optimising the spectral shape of the amplified beam.

The two amplification stages are based on β-barium borate (BBO) crystals in type-I phasematching. We use the walk-off compensation geometry. The choice of non-collinear, and phase-matching angles, and the pump intensity in both stages were guided by numerical simulations carried out with the code SISYFOS (simulation system for optical science) [30, 31]. Our first stage is pumped by 12 W (120 μJ/pulse) pulses at an intensity of 100 GW cm^{-2}. The seed pulses are amplified from 250 pJ/pulse to 1.2 W (12 μJ/pulse). The gain is around 48 000 and the pump-to-seed conversion efficiency is 10%. The second stage is pumped by 96 W (960 μJ) at an intensity of 50 GW cm^{-2}. The seed pulses are amplified to a maximum of 24.2 W (242 μJ/pulse). Here, the gain is 20.2, and the conversion efficiency 24%.

In both amplification stages, the non-collinear angle was the so-called 'magic angle', where the projection of the group velocity of the idler onto the direction of the signal beam equals the group velocity of the signal. This configuration enables broad amplification bandwidth and minimises angular

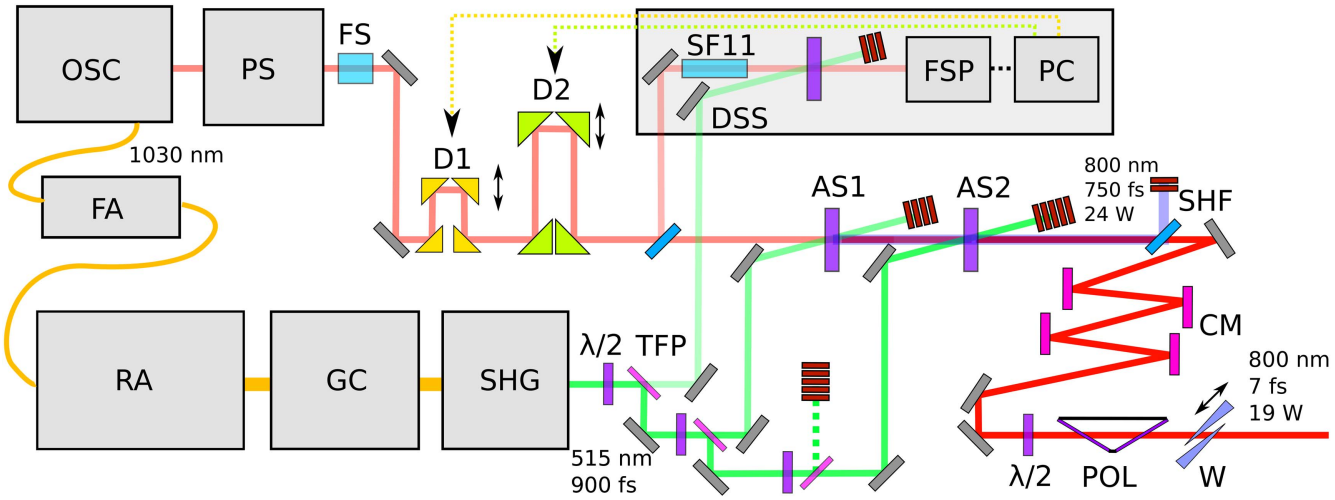

Figure 1. Schematic layout of the NOPCPA system. OSC oscillator, PS pulse shaper, FS fused silica bulk stretcher, FA fibre amplifier, RA regenerative amplifier, GC grating compressor, SHG, second harmonic generation module, D1 piezo driven low mass fast delay stage, D2 long range delay stage, DSS delay stabilisation system, SF11 50 mm SF11 bulk stretcher, FSP fibre coupled spectrometer, PC personal computer, AS1 nopa amplification stage 1, AS2 nopa amplification stage 2, SHF parasitic second harmonic filter, CM chirped mirror compressor, $\lambda/2$ broadband half-wave plate, POL broadband polariser, W thin fused silica wedges for dispersion fine tuning. For a detailed description, please refer to section 2 in the text.

dispersion [32]. The amplified spectrum ranges from 670 to 1050 nm, where the lower bound is dictated by the phase-matching and the upper bound by the output of the seed oscillator. Optimum temporal compression is achieved by a combination of chirped mirrors (Laser Quantum DCM11) and a pair of thin fused silica wedges, located after the amplification stages. After initial compression we use the PS to fine-tune the third and fourth order dispersion terms. Typically, we achieve compression to pulses with a duration from 6.3 to 7.5 fs dependent on the configuration of the seed oscillator and the time delays and phase-matching angles in the amplification stages. After losses in the chirped mirror compressor, the glass wedges, a broadband attenuator and second harmonic rejector, the system delivers pulses with average powers of up 19 W (190 μJ). A more detailed description of the laser system is given in [28]. The pulse energy of this laser system is sufficient to efficiently drive HHG in loose focusing geometry. Therefore, this laser system can directly replace Ti:sapphire plus post-compression driver lasers in existing attosecond pump-probe beamlines with only minor modifications. Coupled to a reaction microscope this will enable high signal-to-noise attosecond pump-probe experiments.

3. Spatio-temporal characterisation

3.1. Introduction

With the rapid advances in laser pulse generation with ever shorter durations, more and more sophisticated laser pulse metrology methods had to be developed going well beyond the simple autocorrelation [33]. Modern pulse metrology methods are able to retrieve the complete electric field of laser pulses down to few-cycle durations. The most prominent techniques are frequency-resolved optical gating (FROG) and spectral phase interferometry for direct electric field reconstruction (SPIDER). The field of ultrafast metrology is still evolving to keep up with the advances in short laser pulse generation, with developments towards more complex pulse metrology and also simplification of devices, a recent example of the latter being the dispersion scan technique [34].

Usually space-time couplings in laser pulses are ignored. I. e. it is assumed that the complex electric field of a laser pulse can be written as the product of a spatially dependent field and a temporally dependent field $E(x, y, t) = E(x, y)\, E(t)$. Most pulse characterization techniques are designed to measure the electric field of the beam at one spatial point $E(x_0, y_0, t)$ or average over the entire or a sub-sample of the beam selected by an aperture. The absence of space-time couplings is expected for most laser systems with clean spatial modes. E.g. the beams emitted from Ti:sapphire lasers and well-aligned hollow fibre compressors are usually space-time coupling free. Space-time couplings can however occur upon angular misalignments or imperfect mode-match of the input beam to the fundamental fiber mode [35]. Even for well-aligned hollow fiber compressors, simple aperturing will change the spectral shape dramatically (radial λ^2 dependence) and lead to erroneous pulse characterisation with spatially integrating techniques. In case of the non-collinear interaction geometries in NOPCPA laser systems as introduced in section 2, space-time couplings are unavoidable. We have performed extensive numerical simulations and conclude that space-time couplings are expected in these laser systems [31]. Furthermore, a few recently introduced attosecond pulse gating techniques such as the attosecond lighthouse [36–38] or non-collinear gating of HHG [39, 40] make use of intentional spatio-temporal distortions where $E(x, y, t) \neq E(x, y)E(t)$. Rather, in these systems the electric field is given by $E(x, y, t) = E(x, y, t + \xi_x x + \xi_y y)$ with the spatio-temporal coupling coefficients ξ_x and ξ_y.

The ability to measure STCs is important not only for the optimization of laser sources and experiments, but also for accurate modelling. Most known spatio-temporal pulse characterization techniques rely on interfering the space-time coupled pulse with a known reference pulse or a spatially filtered version of the unknown pulse, and spatially scanning a this probe along x and y. Recent examples include SEA-TADPOLE, where a FROG measurement of a reference pulse is combined with spectral interferometry and an optical fibre is scanned along x and y within the spatial profile of the unknown pulse [41]. A variant of this is STARFISH which follows the same concept as SEA-TADPOLE, but replaces FROG by the dispersion scan (d-scan) technique for characterisation of the reference pulse [42]. The complete retrieval of the optical amplitude and phase using the (k, ω) spectrum (CROAK) technique combines multiple frequency and angle-resolved measurements of the pulse spectrum in the near and far fields with a Gerchberg–Saxton algorithm [43]. The wavefront autocorrelation technique is able to retrieve the pulse duration and some forms of STC [44]. In the shackled FROG technique a single FROG measurement at one selected spatial point is combined with spatial amplitude and phase measurements for a range of selected wavelengths via the Hartmann–Shack method [45] to yield spatio-temporal pulse reconstructions. The HAMSTER method simplifies this concept by employing a programmable acousto optic amplitude and phase filter, which serves as a programmable spectral filter for the wavefront measurements and as a pulse pair generator for the FROG measurement in the beam centre [46]. D-scan has been combined with point diffraction interferometry and Fourier transform spectrometry to characterize sub-8 fs pulses from an oscillator [47]. Pariente *et al* combined the Wizzler technique [48] for temporal pulse measurement with a form of point diffraction interferometry to the space-time characterisation of ultra-intense lasers [49]. All above mentioned methods inherently rely on a stable laser source over the duration of the scanning measurement and require that the temporal reference pulse measurement is performed with exactly the same dispersion compared to the spatial measurement after spatial filtering. This is very difficult to achieve experimentally, especially for few-cycle pulses. One example for a non-scanning single-frame method is STRIPED FISH [50]. However, here the beam is sampled at a number of spatially disjoint points with limited spectral resolution and it is not a zero-additional phase measurement. An excellent review of space-time couplings in ultrafast laser pulses including an overview of spatio-temporal pulse characterisation methods is given in [51]. In light of the specific problems arising when dealing with few-cycle pulses, we will now discuss a pulse characteristion-technique able to perform spatio-temporal measurements in a self-referencing manner with zero-additional phase imposed onto the unknown pulse.

3.2. SEA-F-SPIDER

A particularly powerful technique for the characterization of ultrafast laser pulses is SPIDER [52]. SPIDER enables a direct algebraic pulse reconstruction from the measured data. Furthermore, a one-dimensional unknown electric field $E(x_0, y_0, t)$ is fully described by a one-dimensional data trace $S(x_0, y_0, \omega)$. Therefore, SPIDER is ideally suited to extend the measurements to include spatial information. The combination of SPIDER and additional spatial shearing allowed for the direct space-time characterization of ultrashort optical pulses in the 60 fs range [53, 54]. Spatially-encoded arrangement filter-based SPIDER (SEA-F-SPIDER) is a spatially resolving technique capable of single-shot measurements and can retrieve space-time couplings without an additional spatial shearing interferometer. The ability of SEA-F-SPIDER to reconstruct near-single-cycle and even sub-cycle pulses has been demonstrated previously [7, 55]. Reconstruction of pulse-front distortions (apart from a linear x–t-couplings) by SEA-F-SPIDER has been demonstrated [56]. Recently, this has been extended to also include the linear (pulse-front tilt) STC by adding a correction term to the SPIDER reconstruction routine [57, 58]. In SEA-F-SPIDER, the broadband unknown pulse is non-collinearly sum-frequency mixed with two quasi-monochromatic pulses, usually termed ancilla pulses. Any space-time couplings present in the unknown pulse are copied into the two sum-frequency signal beams. However, due to non-collinear mixing the signal beams also carry a defined amount of angular dispersion, which is removed by the zero-shear calibration procedure (necessary in all spectral shearing methods). However, when one of the two quasi-monochromatic beam's frequency is changed to produce a shear (i.e. the frequencies of ancilla A and ancilla B differ now), the introduced angular dispersion in signal B now differs from the calibration step, which leads to an erroneous pulse front tilt term. This can be taken into account by an extra term $\theta\Omega x/c$ in the SEA-F-SPIDER interferogram:

$$\begin{aligned} S(x, \omega) = {} & |E(x, \omega)|^2 + |E(x, \omega - \Omega)|^2 \\ & + 2|E(x, \omega)|\,|E(x, \omega - \Omega)| \\ & \times \cos[\phi(x, \omega) - \phi(x, \omega - \Omega) + \Delta kx + \theta\Omega x/c]. \end{aligned} \tag{1}$$

The extra term $\theta\Omega x/c$ represents the additional spatial phase gradient resulting from the k-vector change of ancilla B k between calibration and non-zero shear. Δkx is given by the crossing angle of the two sum-frequency beams. The $\theta\Omega x/c$ term has to be calibrated for accurate reconstruction of the pulse-front-tilt. Knowledge of the exact frequencies $\omega_{B,\Omega=0}$ and $\omega_{B,\Omega\neq 0}$ is enabled by the direct spectral filtering approach of the ancilla preparation [59]. SEA-F-SPIDER can characterise the spatio-temporal electric field of unknown laser pulses along one spatial dimension in the x–y-plane.

Figure 2 shows the experimental setup of the SEA-F-SPIDER apparatus used in this work. The beam from the NOPCPA laser system is attenuated by a broadband half-wave retarder and thin-film polariser combination. We use a periscope P which can be configured to either send the beam in its original orientation or cause a 90°rotation. This way we can analyse the horizontal and vertical planes of the laser beam. After entering the device a small fraction of the unknown pulse is picked off by an uncoated beam sampler

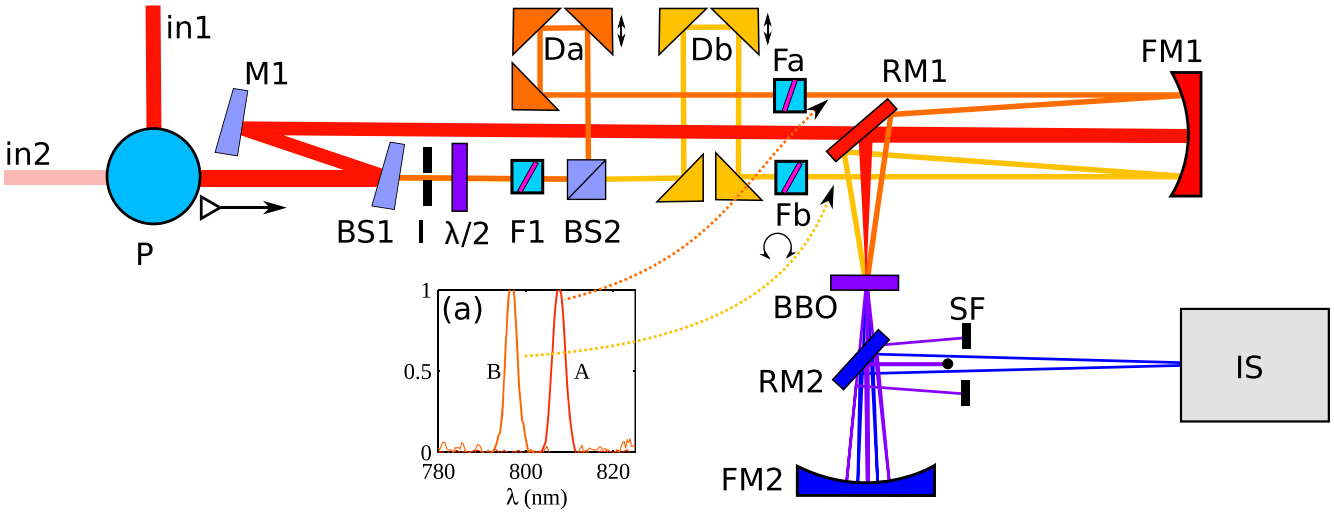

Figure 2. Setup of the SEA-F-SPIDER for spatio-temporal characterisation. As SEA-F-SPIDER measures one spatial slice $E(x, t)$, the periscope P can be configured to characterise the beam in the horizontal x-plane to retrieve $E(x, t)$ or in the vertical y-plane to retrieve $E(y, t)$. Please refer to section 3.2 in the text for a detailed description of the SEA-F-SPIDER setup.

BS1. Subsequently, the unknown pulse experiences no dispersion apart from linear propagation in air until it enters the nonlinear crystal. The transmission of BS1 is used to create the two ancilla beams. The beam is first apertured to reduce the ancilla beam size leading to a uniform field at the focus. Aperturing is sufficient to remove space-time couplings and leads to uniform spatio-temporal ancilla fields at focus for sum-frequency mixing with the unknown pulse. We checked this experimentally and also numerically. For an original beam size of 6 mm, an aperture size of 1 mm is sufficient. If available an external ancilla beam can also be used [35, 60]. But in this work, we derive the ancilla from the NOPCPA beam that enters the SEA-F-SPIDER. A half-wave plate ($\lambda/2$) rotates the ancilla polarization to enable type-II upconversion in the crystal BBO ($\theta = 43°$, $L = 10$ μm). The phase-matching bandwidth spans from 450 nm to well upwards of 1.5 μm and is fairly flat accross the bandwidth of the NOPCPA. The ancilla beam is divided into two beams A and B with adjustable delay lines Da and Db. These allow to adjust the temporal overlap with the test pulse but only have to be set once upon initial alignment of the device. Fa and Fb are narrowband bandpass filters (Semrock MaxLine LL01-808) which directly produce quasi-monochromatic ancilla beams in transmission. Thus no temporal stretching is required. Typical transmission spectra are displayed in figure 2 as inset (a). The bandpass filters Fa and Fb have some leakage at wavelengths below 600 nm. We use a long-pass filter F1 (Thorlabs, FGL665) to eliminate this leakage. Simple rotation of the bandpass filters Fa and Fb allows setting the ancilla frequencies. Servo motors (Hitec HS-5485HB) are used to automate this. After initial calibration of transmission versus motor position fully automated data acquisition is possible. The filters are mounted such that the rotation axis is parallel to the plane of beam separation. In our case the filters rotate out of the drawing plane in figure 2. This avoids a change in Δkx with angle. The three beams, ancilla A, TP, and ancilla B are aligned to be parallel and focused into the BBO crystal by focusing mirror FM1 ($f = 300$ mm). For perfectly collimated beams, the actual waist coincides with the geometric focus of FM1. FM1 can also be translated to adjust for non-collimated beams. It should be noted here that we measure the pulse at focus. As most experiments are performed at focus this is preferable over other techniques that measure in the collimated beam (see section 3.1). For this work, we measure the beam at focus inside the SEA-F-SPIDER device. For *in situ* measurement e.g. in a vaccum system, it would be possible to create the two ancilla beams outside the vacuum chamber and create the SEA-F-SPIDER sum-frequency signal beams *in situ* at the exact location where the experiment is performed. The signal beams can then be sent to an imaging spectrometer outside vacuum for detection of the SEA-F-SPIDER interferograms. When measuring not perfectly collimated beams were-adjust the ancilla beams to be slightly non-parallel so they meet again in the waist of the unknown pulse. A webcam (not shown in figure 2) is used to monitor and optimise the beam overlap in the crystal plane. After mixing of the two ancilla beams and the unknown pulse in the BBO crystal, the two SPIDER sum-frequency signal beams are spatially isolated by spatial filter (SF). As the two SPIDER beams carry angular dispersion due to the non-collinear mixing of a broadband with a quasi-monochromatic pulse, accurate re-imaging onto the imaging spectrometer IS is necessary. For this FM2 ($f = 150$ mm) is positioned to form a magnified image of the crystal plane onto the slit of IS. The imaging spectrometer itself has to ensure stigmatic imaging of the slit onto the detector. Standard Czerny-Turner spectrometers do not achieve this. Commercial solutions based on Czerny-Turner designs with a Schmidt corrector are now available, but we use a home-built solution based on astigmatism compensation by divergent illumination of the grating in a modified folded Czerny-Turner configuration [61]. Finally, the spatially resolved and spectrally dispersed signal is recorded on a CCD camera with good quantum efficiency and UV response (pco.ultraviolet, PCO AG). Note that the

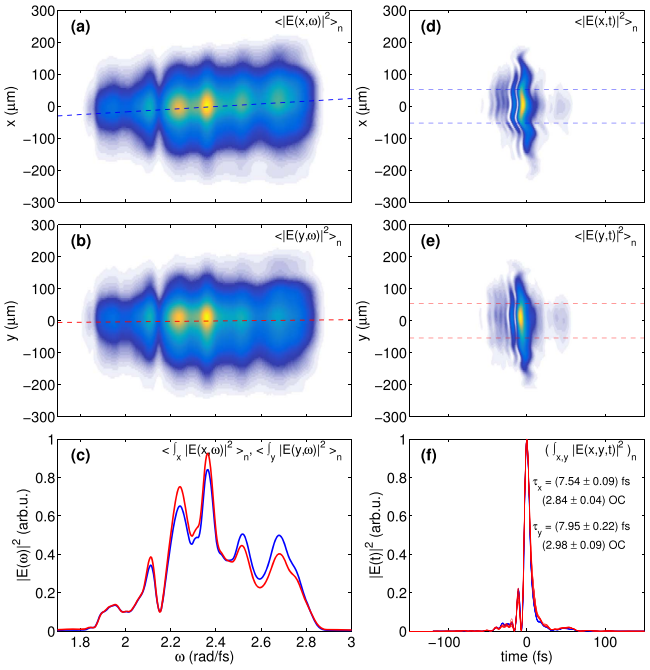

Figure 3. Spatio-spectral and spatio-temporal characterisation of the NOPA output with the second stage unpumped.

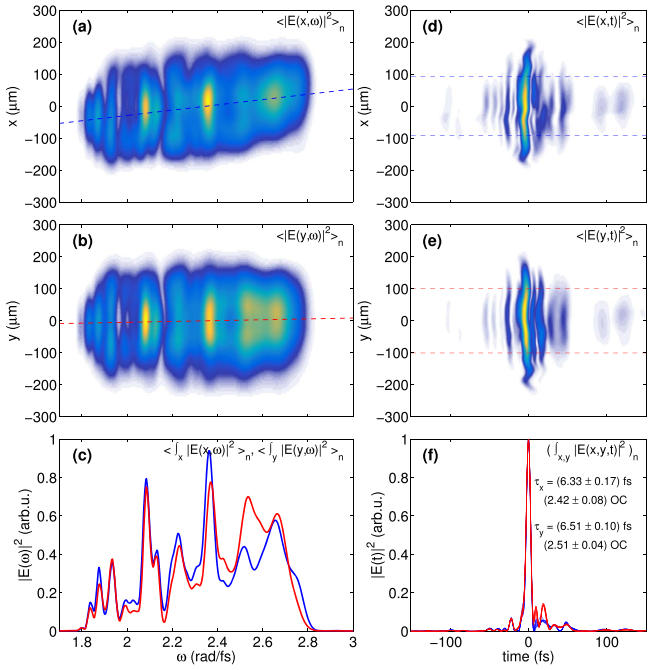

Figure 4. Spatio-spectral and spatio-temporal characterisation of the NOPA output at full power.

spatial interference fringes occur in the plane of the beam crossing angle (in-paper plane in figure 2). As the imaging spectrometer is built horizontally with a vertical slit we use a small periscope in front of the entrance slit of IS (not shown) to rotate the crossing beams so that the crossing is now parallel to the slit.

Before operation, a calibration trace at $\Omega = 0$ is recorded. The fringes of this trace are flat and allow the extraction of Δkx. For measurements we make use of the multiple-shearing algorithm [62]. We use spectral shears Ω of 10 and 50 mrad fs^{-1} in this work. The small shear allows the retrieval of small high frequency features in the phase, and the large shear introduces a large signal-to-noise correction, as well as allows to jump over spectral holes [63].

3.3. Spatio-temporal measurements of the NOPCPA system

To characterise the 24 W output of our NOPCPA laser system we attenuate the beam by means of a combination of a broadband half-waveplate and a thin-film polariser. We typically send 500 mW (5 μJ/pulse) to the SEA-F-SPIDER device. We sequentially acquire SEA-F-SPIDER data for the horizontal beam direction, and for the vertical beam direction in order to retrieve $E(x, y_0, t)$ and $E(x_0, y, t)$ independently, by reconfiguring the periscope P in figure 2. Future improvements might include a continuous beam rotation by an all reflective Dove prism arrangement. Note that even though SEA-F-SPIDER is capable of single-shot measurements we average over multiple laser shots, as the laser repetition rate is 100 kHz.

Figure 3 shows the SEA-F-SPIDER characterisation of the first stage of the NOPCPA amplifier. After sending the few-cycle seed beam through the entire system and optimising the pulse compression at full power we turned off the pump of stage two (see figure 1). Figure 3(a) shows the spatio-spectral distribution $|E(x, \omega)|^2$ in the horizontal x-plane. In our configuration of NOPA and SEA-F-SPIDER, this corresponds to the walk-off plane, i.e. the plane defined by the crossing angle of the pump and seed beams in the NOPA. The image displayed in (a) is the average over 25 subsequent measurements $\langle |E(x, \omega)|^2 \rangle_n$. In figure 3(d), the corresponding spatio-temporal pulse is shown. SEA-F-SPIDER retrieved the full electric field of the laser pulses, but for better visibility we show the intensity distribution $\langle |E(x, t)|^2 \rangle_n$. Figures 3(b) and (e) show the spatio-spectral and spatio-temporal profiles $\langle |E(y, \omega)|^2 \rangle_n$ and $\langle |E(y, t)|^2 \rangle_n$ for the vertical plane. Apart from minor pulse front distortions the pulses are reasonably clean. We are still investigating the origin of the small wavering spatio-temporal distortions seen especially in figure 3(d). For the x-plane a clear spatial chirp is visible (see figure 3(a)), which corresponds to angular dispersion in the collimated beam. In (c), we show the spatially integrated spectra. Apart from minor differences the spectra are virtually identical for the horizontal (blue line) and vertical beam axis (red line). In figure 3(f), we show temporal profiles spatially integrated over the spatial FWHM of the beam in x and y. Here we plot the entire ensemble of 25 measurements. The pulse duration in the horizontal x-plane is 7.54 ± 0.09 fs, which corresponds to 2.84 ± 0.04 optical cycles (OC). In the vertical plane, the FWHM pulse duration is evaluated to be 7.95 ± 0.22 fs (2.98 ± 0.09 OC). A slight negative cubic phase as a result of the now missing contribution of the parametric phase in the unpumped stage 2 is visible.

Figure 4 shows the SEA-F-SPIDER characterisation of the amplified beam with both amplification stages at full pump power. The organisation of the figures is the same as

before in figure 3. The spatio-spectral distribution in the *y*-plane is almost spatial chirp free, whereas we can again identify a spatial chirp in the *x*-plane. The spatio-temporal profiles $\langle|E(x, t)|^2\rangle_n$ and $\langle|E(y, t)|^2\rangle_n$ show only minor pulse front distortions but are free from major pulse front tilts. The spectra are now more structured due to saturation effects and the onset of back-conversion, but apart from the spatial chirp of $\langle|E(x, \omega)|^2\rangle_n$ spatially very symmetric. The dent at around 2.0 rad fs^{-1} in $\langle|E(x, \omega)|^2\rangle_n$ (shown in figure 4(a)) being an exception. The temporal stability is again excellent as evidenced by the 25 subsequent measurements shown in figure 4(f). The FWHM pulse durations are 6.33 ± 0.17 fs (2.42 ± 0.08 OC) for the horizontal, and 6.51 ± 0.10 fs (2.51 ± 0.04 OC) for the vertical beam axis. Compared to the stage one-only measurements shown in figure 3(f), it is striking that the post-pulse structure is slightly different for the two beam axes, which only underlines the importance of spatially resolving, or full spatio-temporal pulse characterisation measurements as we have shown here.

4. Conclusion

In conclusion, we have presented a 100 kHz, 24 W sub-3-cycle laser system capable of driving next generation attosecond sources. We have shown that SEA-F-SPIDER is a convenient single-shot capable method to elucidate the spatio-temporal structure of few-cycle laser pulses amplified in NOPCPAs. Our results illustrate the need for spatio-temporal pulse characterisaton technology to enable the optimisation of these emerging laser systems and the delivery of high fidelity pulses for experiments. Future work will focus on the extension from measurements along one spatial slice of the beam $E(x, y_0, t)$ or $E(x_0, y, t)$ to allow access to the full field $E(x, y, t)$ by integrating hyperspectral imaging technology into the SEA-F-SPIDER device.

Acknowledgments

We are grateful to Achut Giree and Gunnar Arisholm for numerical simulations of the NOPCPA laser system, Dane Austin for useful discussions, and Roman Peslin and Christoph Reiter for technical assistance.

Funding

This work was supported by the European Union through the FP7 Marie Curie EID project JMAP (grant agreement no. 316687), Horizon 2020 program Laserlab Europe (grant agreement no. 654148).

ORCID iDs

Tobias Witting https://orcid.org/0000-0002-2512-1840
Federico J Furch https://orcid.org/0000-0002-8444-7162
Marc J J Vrakking https://orcid.org/0000-0002-3249-1663

References

[1] Brabec T and Krausz F 2000 *Rev. Mod. Phys.* **72** 545–91
[2] Krausz F and Ivanov M 2009 *Rev. Mod. Phys.* **81** 163
[3] Nisoli M, Silvestri S D, Svelto O, Szipöcs R, Ferencz K, Spielmann C, Sartania S and Krausz F 1997 *Opt. Lett.* **22** 522–4
[4] Okell W A *et al* 2013 *Opt. Lett.* **38** 3918–21
[5] Bohman S, Suda A, Kanai T, Yamaguchi S and Midorikawa K 2010 *Opt. Lett.* **35** 1887–9
[6] Malvache A, Chen X, Durfee C G, Jullien A and Lopez-Martens R 2011 *Appl. Phys.* B **104** 5–9
[7] Balciunas T, Fourcade-Dutin C, Fan G, Witting T, Voronin A A, Zheltikov A M, Gerome F, Paulus G G, Baltuska A and Benabid F 2015 *Nat. Commun.* **6** 6117
[8] Jacqmin H, Mercier B, Jullien A and Lopez-Martens R 2016 *Appl. Phys.* B **122** 218
[9] Sansone G *et al* 2006 *Science* **314** 443–6
[10] Hentschel M, Kienberger R, Spielmann C, Reider G A, Milosevic N, Brabec T, Corkum P, Heinzmann U, Drescher M and Krausz F 2001 *Nature* **414** 509–13
[11] Fabris D, Witting T, Okell W A, Walke D J, Matia-Hernando P, Henkel J, Barillot T R, Lein M, Marangos J P and Tisch J W G 2015 *Nat. Photon.* **9** 383–7
[12] Zhao K, Zhang Q, Chini M, Wu Y, Wang X and Chang Z 2012 *Opt. Lett.* **37** 3891–3
[13] Ganeev R A, Witting T, Hutchison C, Frank F, Tudorovskaya M, Lein M, Okell W A, Zar A, Marangos J P and Tisch J W G 2012 *Opt. Express* **20** 25239–48
[14] Kienberger R, Chang Z and Nam C H 2012 *J. Phys. B: At. Mol. Opt. Phys.* **45** 070201
[15] Drescher M, Hentschel M, Kienberger R, Uiberacker M, Yakovlev V, Scrinzi A, Westerwalbesloh T, Kleineberg U, Heinzmann U and Krausz F 2002 *Nature* **419** 803–7
[16] Barillot T R, Matia-Hernando P, Greening D, Walke D J, Witting T, Frasinski L J, Marangos J P and Tisch J W G 2017 *Chem. Phys. Lett.* **683** 38–42
[17] Calegari F *et al* 2014 *Science* **346** 336–9
[18] Cavalieri A L *et al* 2007 *Nature* **449** 1029–32
[19] Neppl S *et al* 2015 *Nature* **517** 342–6
[20] Okell W A *et al* 2015 *Optica* **2** 383–7
[21] Ullrich J, Moshammer R, Dorn A, Dörner R, Schmidt L P H and Schmidt-Böcking H 2003 *Rep. Prog. Phys.* **66** 1463
[22] Sabbar M, Heuser S, Boge R, Lucchini M, Gallmann L, Cirelli C and Keller U 2014 *Rev. Sci. Instrum.* **85** 103113
[23] Hädrich S *et al* 2016 *Opt. Lett.* **41** 4332–5
[24] Prinz S *et al* 2015 *Opt. Express* **23** 1388–94
[25] Matyschok J *et al* 2013 *Opt. Express* **21** 29656–65
[26] Rothhardt J, Demmler S, Hädrich S, Limpert J and Tünnermann A 2012 *Opt. Express* **20** 10870–8
[27] Furch F J, Giree A, Morales F, Anderson A, Wang Y, Schulz C P and Vrakking M J J 2016 *Opt. Express* **24** 19293–310
[28] Furch F J, Witting T, Giree A, Luan C, Schell F, Arisholm G, Schulz C P and Vrakking M J J 2017 *Opt. Lett.* **42** 2495–8
[29] Prinz S, Häfner M, Schultze M, Teisset C Y, Bessing R, Michel K, Kienberger R and Metzger T 2014 *Opt. Express* **22** 31050–6
[30] Arisholm G 1997 *J. Opt. Soc. Am.* B **14** 2543–9
[31] Giree A, Mero M, Arisholm G, Vrakking M J J and Furch F J 2017 *Opt. Express* **25** 3104–21
[32] Bromage J, Dorrer C and Zuegel J D 2010 *Opt. Lett.* **35** 2251–3
[33] Diels J C, van Stryland E and Benedict G 1978 *Opt. Commun.* **25** 93–5

[34] Miranda M, Fordell T, Arnold C, L'Huillier A and Crespo H 2012 *Opt. Express* **20** 688–97
[35] Austin D R, Witting T, Weber S J, Ye P, Siegel T, Mata-Hernando P, Johnson A S, Tisch J W and Marangos J P 2016 *Opt. Express* **24** 24786
[36] Wheeler J A, Borot A, Monchoc S, Vincenti H, Ricci A, Malvache A, Lopez-Martens R and Qur F 2012 *Nat. Photon.* **6** 829–33
[37] Kim K T, Zhang C, Ruchon T, Hergott J F, Auguste T, Villeneuve D M, Corkum P B and Qur F 2013 *Nat. Photon.* **7** 651–6
[38] Qur F *et al* 2014 *J. Phys. B: At. Mol. Opt. Phys.* **47** 124004
[39] Heyl C M, Bengtsson S N, Carlstrm S, Mauritsson J, Arnold C L and L'Huillier A 2014 *New J. Phys.* **16** 052001
[40] Louisy M *et al* 2015 *Optica* **2** 563
[41] Bowlan P, Gabolde P, Shreenath A, McGresham K, Trebino R and Akturk S 2006 *Opt. Express* **14** 11892–900
[42] Alonso B, Miranda M, Sola I J and Crespo H 2012 *Opt. Express* **20** 17880–93
[43] Bragheri F *et al* 2008 *Opt. Lett.* **33** 2952
[44] Grunwald R, Neumann U, Griebner U, Reimann K, Steinmeyer G and Kebbel V 2003 *Opt. Lett.* **28** 2399
[45] Rubino E, Faccio D, Tartara L, Bates P K, Chalus O, Clerici M, Bonaretti F, Biegert J and Di Trapani P 2009 *Opt. Lett.* **34** 3854
[46] Cousin S L, Bueno J M, Forget N, Austin D R and Biegert J 2012 *Opt. Lett.* **37** 3291–3
[47] Miranda M, Kotur M, Rudawski P, Guo C, Harth A, L'Huillier A and Arnold C L 2014 *Opt. Lett.* **39** 5142
[48] Moulet A, Grabielle S, Cornaggia C, Forget N and Oksenhendler T 2010 *Opt. Lett.* **35** 3856–8
[49] Pariente G, Gallet V, Borot A, Gobert O and Qur F 2016 *Nat. Photon.* **10** 547–53
[50] Guang Z, Rhodes M, Davis M and Trebino R 2014 *J. Opt. Soc. Am.* B **31** 2736
[51] Akturk S, Gu X, Bowlan P and Trebino R 2010 *J. Opt.* **12** 093001
[52] Iaconis C and Walmsley I A 1998 *Opt. Lett.* **23** 792–4
[53] Dorrer C, Kosik E M and Walmsley I A 2002 *Opt. Lett.* **27** 548–50
[54] Dorrer C, Kosik E and Walmsley I 2002 *Appl. Phys. B: Lasers Opt.* **74** s209–17
[55] Witting T, Frank F, Arrell C A, Okell W A, Marangos J P and Tisch J W G 2011 *Opt. Lett.* **36** 1680–2
[56] Witting T, Weber S J, Tisch J W G and Marangos J P 2012 *Opt. Express* **20** 27974–80
[57] Wyatt A and Walmsley I 2009 Analysis of space-time coupling in SEA-SPIDER measurements *European Conf. on Lasers and Electro-Optics 2009. CLEO Europe 2009* p 1
[58] Witting T, Austin D R, Barillot T, Greening D, Matia-Hernando P, Walke D, Marangos J P and Tisch J W G 2016 *Opt. Lett.* **41** 2382–5
[59] Witting T, Austin D R and Walmsley I A 2009 *Opt. Lett.* **34** 881–3
[60] Fan G, Balinas T, Fourcade-Dutin C, Haessler S, Voronin A A, Zheltikov A M, Grme F, Benabid F, Baltuka A and Witting T 2016 *Opt. Express* **24** 12713–29
[61] Austin D R, Witting T and Walmsley I A 2009 *Appl. Opt.* **48** 3846–53
[62] Austin D R, Witting T and Walmsley I A 2009 *J. Opt. Soc. Am.* B **26** 1818–30
[63] Austin D R, Witting T and Walmsley I A 2010 *Opt. Lett.* **35** 1971–3